Point defects in hexagonal BN, BC_3 and BC_xN compounds studied by x-ray absorption near-edge structure

Ignacio Caretti[a] and Ignacio Jiménez
Instituto de Ciencia de Materiales de Madrid (ICMM-CSIC), Campus de Cantoblanco, 28049 Madrid, Spain

(Received 14 December 2010; accepted 22 May 2011; published online 21 July 2011)

The generation of point defects in highly oriented pyrolytic boron nitride (HOPBN) after Ar^+ ion bombardment in ultrahigh vacuum and subsequent exposure to air was studied by angle-resolved x-ray absorption near edge structure (XANES). The pristine HOPBN showed well-oriented boron nitride (BN) basal planes parallel to the surface, with a negligible amount of defects. Amorphization of the BN structure took place after Ar^+ sputtering, as indicated by the broadening of the XANES spectra and significant decrease of the characteristic π^* states. Following air exposure, the XANES analysis revealed a spontaneous reorganization of the sample structure. The appearance of four new B1*s* π^* excitonic peaks indicates an oxygen decoration process of the nitrogen vacancies created by ion bombardment. A core-level shift model is presented to support this statement. This model is successfully extended to the case of oxygen substitutional defects in hexagonal BC_3 and BC_xN $(0 < x < 4)$ materials, which can be applied to any B-based sp^2-bonded honeycomb structure. © *2011 American Institute of Physics*. [doi:10.1063/1.3602996]

I. INTRODUCTION

Hexagonal boron nitride (*h*-BN) is a thermally and chemically highly stable wide-band-gap (~4–7 eV)[1] material, whose optical[1–8] and thermoelectrical[9–12] properties strongly depend upon the occurrence and nature of point defects within its sp^2-bonded honeycomb structure. Many of the technological uses of *h*-BN are therefore subject to the identification and quantification of the type and concentration of such defects, which ultimately determine the electronic structure of the material.

Bulk single crystals of *h*-BN are usually synthesized by high-pressure/high-temperature (HP/HT) methods[1] or, since recently, at atmospheric pressures.[3,13] Highly oriented polycrystalline *h*-BN bulk samples are also obtained by compression-annealed pyrolysis.[14] Furthermore, CVD[15–20] and PVD[10,15,21–26] techniques have been extensively employed to grow *h*-BN thin films with different degrees of structural disorder. With the advent of nanotechnology, a number of BN nanostructures such as nanotubes, nanoribbons or fullerenes have been successfully produced by chemical or physical methods.[27]

Typically, a reduced number of defects and impurities are present in *h*-BN bulk crystals. In contrast, *h*-BN thin films and BN nanomaterials are commonly synthesized outside the thermodynamic equilibrium through processes involving energetic particles (e.g., ions or electrons), what leads to more defective structures. For example, plasmas or directional bombardment of N_2^+ and/or Ar^+ ions are often used for *h*-BN thin film deposition[10,15,17,18,20,22–26] and BN nanotube formation.[27,28] Also, nanoribbons[29,30] and fullerenes[28,31] of BN have been produced with the help of electron beam irradiation. Point defects are thus readily formed as result of the regular synthesis processes in an uncontrolled way, but they can be intentionally generated to modify the characteristics of BN, for instance by irradiation.[25,26] In this sense, the production of well-controlled defect arrangements is of great importance for the fabrication of BN structures with defined properties.

Regarding the optical properties, the observation of UV lasing characteristics in an *h*-BN single crystal[1] triggered significant research on this material as a possible candidate for light-emitting devices. Since then, several photo- and cathodoluminescence studies[3–5,7,8,32–34] have been published in an effort to understand the electronic and optical properties of *h*-BN. According to these reports, exciton formation, impurities and defects are responsible for *h*-BN luminescence, due to the formation of acceptor and donor levels in the band-gap. In general, the UV emission spectrum of *h*-BN exhibits two bands (around ~4 eV and ~5.5 eV), more or less structured depending on the crystallinity. The former is commonly assigned to vacancies, and C and/or O impurities; the latter comprises free exciton and exciton-bound-to-defects emission. However, up until now, the origin of these emission bands is still a matter of controversy. Thus, the investigation of point defects and the excitonic structure of *h*-BN plays a crucial role in the development of future optoelectronic applications.

With respect to electrical properties, *h*-BN is an interesting candidate for high-temperature electronic devices. However, the dielectric behavior of *h*-BN with temperature has not been sufficiently studied. Recently, some work have investigated the effect of point defects on the high-temperature conductivity and dielectric loss of *h*-BN.[9–12] For bulk *h*-BN, the increase in the conductivity and subsequent dielectric loss with temperature was linked to thermal excitation of B vacancies and oxygen ionic substitutional and midplane defects.[9,12] Besides, a larger amount of defects was related to a higher conductivity in turbostratic BN thin films,[10] and to a larger activation energy in Zn-doped *h*-BN compared to *c*-BN thin films.[11]

[a]Electronic mail: caretti@icmm.csic.es.

According to the above exposed, it is clear that the analysis of point defects (i.e., B and N vacancies and interstitials, as well as impurities) is a cornerstone in the comprehension and control of the properties of sp^2-bonded BN materials. In this direction, a number of theoretical and experimental works have been devoted to the study of point defect formation in *h*-BN and related nanostructures. In 1974, Katzir *et al*.[35] were the first to carry out a thorough study of point defects in *h*-BN by electron paramagnetic resonance (EPR), pointing out the role of impurities and vacancies in the thermoluminescent properties and the formation of *F*-centers by electron irradiation. In 1997, Jiménez *et al*.[26] identified the formation of point defects in boron nitride by x-ray absorption near edge spectroscopy (XANES). In that paper, the authors explored the use of XANES for the identification and quantification of point defects, and shown the presence of different N-void defects and N interstitials formed during the growing process of *h*-BN thin films, or due to ion implantation. Among the experimental evidence, they reported that, additionally to the characteristic B($1s \rightarrow \pi^*$) excitonic transition of *h*-BN at ~192.0 eV from a B-N_3 trigonal bonding environment, three new excitonic π^* peaks were observed in the B1*s* x-ray absorption edge at ~192.6 eV, ~193.2 eV and ~194.0 eV. Those peaks, labeled in that work as *X*, *Y* and *Z*, were assigned to B surrounded by 1, 2 and 3 N-void defects, respectively. Notice that the term "nitrogen vacancy" was intentionally shunned because these N vacant sites might be occupied by substitutional impurities like C or O. In fact, these or other impurity defects are likely to happen at the surface of defective *h*-BN structures. In that case, the three localized excitonic levels at higher energy (*X*-*Z* peaks) would arise from the chemical shift of the core levels sensed by XANES.

In connection to this, many other groups have reported the presence of these N-defect related π^* excitonic transitions in the B1*s* XANES spectrum of sp^2-hybridized BN compounds and nanostructures. However, no consensus has been achieved yet with regard to the interpretation given to these π^* peaks. On the basis of theoretical calculations, Pavlychev *et al*.[36] claimed that these extra π^* resonance features, in the B1*s* photoabsorption spectrum of *h*-BN powder crystals, were due to displacements of the core-excited B atoms out of the basal plane. Broad π^* excitonic states were also observed in the same energy region as *X*-*Z* by Shimoyama *et al*. in epitaxial boron nitride films on Ni(111), and attributed in this case to the interaction with the Ni substrate.[37,38] Recently, a wider π^* excitonic distribution (189–195 eV) with resolved *X*-*Z* peaks was detected after low-energy Ar^+ or $N_2{}^+$ ion-bombardment of *h*-BN crystalline powder attached to a carbon tape.[39–41] The *X*-*Z* peaks were assigned to a gradual increment of N-vacancies around the B atoms.[25,26] A similar explanation was given in a XANES study of BN nanotubes, while the intense *Z* peak was suggested to originate from unreacted boron oxide used in the preparation procedure.[42] In another XANES analysis of BN bamboo-like nanotubes and nanothorns,[43] these *X*-*Z* π^* transitions were assigned to the same N-void defects, but occupied by B in antisite positions. Furthermore, Preobajenski *et al*.[44] argued that peaks *X* and *Y* were linked to Co-*h*-BN bonds in a Co intercalated *h*-BN nanomesh, while peak *Z* was attributed to B-O bonds. Finally, similar π^* excitonic peaks are detected in the B1*s* XANES spectrum of hexagonal-like boron carbide (*h*-BC_3)[45] and boron carbonitride (*h*-BC_xN) materials.[46,47] Altogether, it is clear that a great deal of information is contained in the excitonic peaks within the B1*s* XANES spectrum of *h*-BN, but their origin still remains a matter of debate.

Interestingly, to our knowledge, no analogous B vacancy-related defects have been observed so far in BN by XANES, what indicates a preferential formation of N-void defects instead of *B* ones. Supporting this observation, theoretical calculations predict a higher formation energy for B monovacancies compared to N.[48,49] In contrast, high-resolution transmission electron microscopy (HRTEM) studies have reported recently the formation of point defects in *h*-BN single-layers, thinned down with a high-energy electron beam.[29,30,50,51] Strikingly, it seems that B vacancies are preferentially formed to N vacancies. It is obvious that, at present, the nature and formation of point defects in *h*-BN structures is an open unresolved subject on which rely many of its promising properties.

In this paper, we bring new light to the identification of point defects in *h*-BN, *h*-BC_3 and *h*-BC_xN ($0 < x < 4$) compounds using XANES as characterization technique. We have exploited its chemical selectivity, as well as the sensitivity to sample orientation and hybridization, to study a highly oriented pyrolytic *h*-BN (HOPBN) sample with a well-defined orientation of the basal planes and negligible concentration of native defects. We present the angular resolved XANES analysis of HOPBN in three stages: (i) pristine sample, (ii) after low-energy ion-bombardment with Ar^+ in ultrahigh vacuum, and (iii) after subsequent exposure to air. Our results demonstrate that the B1*s* excitonic peaks observed in many of the reported XANES spectra of sp^2-bonded BN materials can be unequivocally described by oxygen decorated N vacancies. A core-level shift model based on the different electronegativities of the ligands confirms this interpretation. This model is extended here to *h*-BC_3 and *h*-BC_xN ($0 < x < 4$) compounds in a consistent way, allowing us to identify the bonding environments related to the π^* resonant peaks in the B1*s* absorption edge.

II. EXPERIMENT

The analyzed HOPBN, with dimensions about 5×5 mm^2, consists of an assembly of microcrystals with parallel *c* axes (measured mosaic spread is less than 1°), but randomly oriented in the basal plane.[52] The BN stoichiometry of the sample was assessed by XANES and x-ray energy dispersive spectroscopy (XEDS),[53] and compared with crystalline *h*-BN powders of high purity (< 99,9%) as reference.

The full round of XANES measurements on HOPBN were performed sequentially at the bending magnet SA72 beamline of the LURE synchrotron source, in Orsay (France), using the SACEMOR endstation. The spectra were recorded at normal incidence (0°), intermediate (55°) and grazing incidence (75°) of the x-ray beam with respect to the sample surface normal. The x-ray absorption was recorded

in the total electron yield mode by measuring the current drained to ground from the HOPBN sample. The latter was normalized by the signal from a gold-coated metal grid located upstream in the x-ray beam path. Complementary measurements on HOPBN and BCN were performed at the PM4 beamline of the BESSY II synchrotron facility in Berlin (Germany), using the SURICAT endstation.

The XANES spectra of HOPBN were acquired in three different stages. First, the HOPBN was introduced in the preparation chamber and outgassed at 500 °C in order to eliminate oxygen contamination from the surface. The absence of oxygen was verified by looking at the O1*s* x-ray absorption. The measured B1*s* and N1*s* XANES spectra were taken as references of the hereafter called *clean HOPBN* sample. Second, the HOPBN surface was bombarded for 5 mins with 3 keV Ar^+ ions using a current of 20 μA, and the XANES spectra were recorded again. Third, the HOPBN sample was taken outside the vacuum chamber and exposed to air for 5 mins. Then, it was introduced back in the analysis chamber to collect the last set of XANES spectra.

It should be mentioned that due to the highly insulating characteristics of the HOPBN sample, charge accumulation effects played an important role in the acquisition of the XANES.

B1*s* and N1*s* spectra. Once the measurement conditions were set, we let the x-ray beam irradiate the HOPBN until the photocurrent was stable before starting the XANES scan. In this way, the sample remains charged at a constant voltage during the acquisition. Otherwise, the characteristic photoinduced charge-discharge curves were observed when moving from the N1*s* to the B1*s* edge, burying the XANES spectra. Even in the best conditions, the spectra were often noisy, a fact that was intrinsic to the sample and could not be improved with the analysis setup.

For the study of the B1*s* XANES spectra of hexagonal BC_xN compounds we synthesized 5 thin film samples grown on Si(100) by ion beam assisted deposition (IBAD) as described elsewhere.[54]

III. RESULTS AND DISCUSSION

A. The HOPBN experiment – spontaneous reordering of an ion bombarded hexagonal structure

Figure 1 shows the B1*s* and N1*s* XANES spectra of clean HOPBN, Ar^+ sputtered HOPBN and Ar^+ sputtered HOPBN exposed to air, normalized to the same height. The measurements were performed at three different angles in order to monitor the sample anisotropies. XANES spectra from two reference samples are also included for comparison purposes: a polycrystalline *h*-BN powder (bottom panels) and an *h*-BN thin film grown at 500 °C by pulsed laser deposition (PLD) of BN, with simultaneous N_2^+ ion assistance at

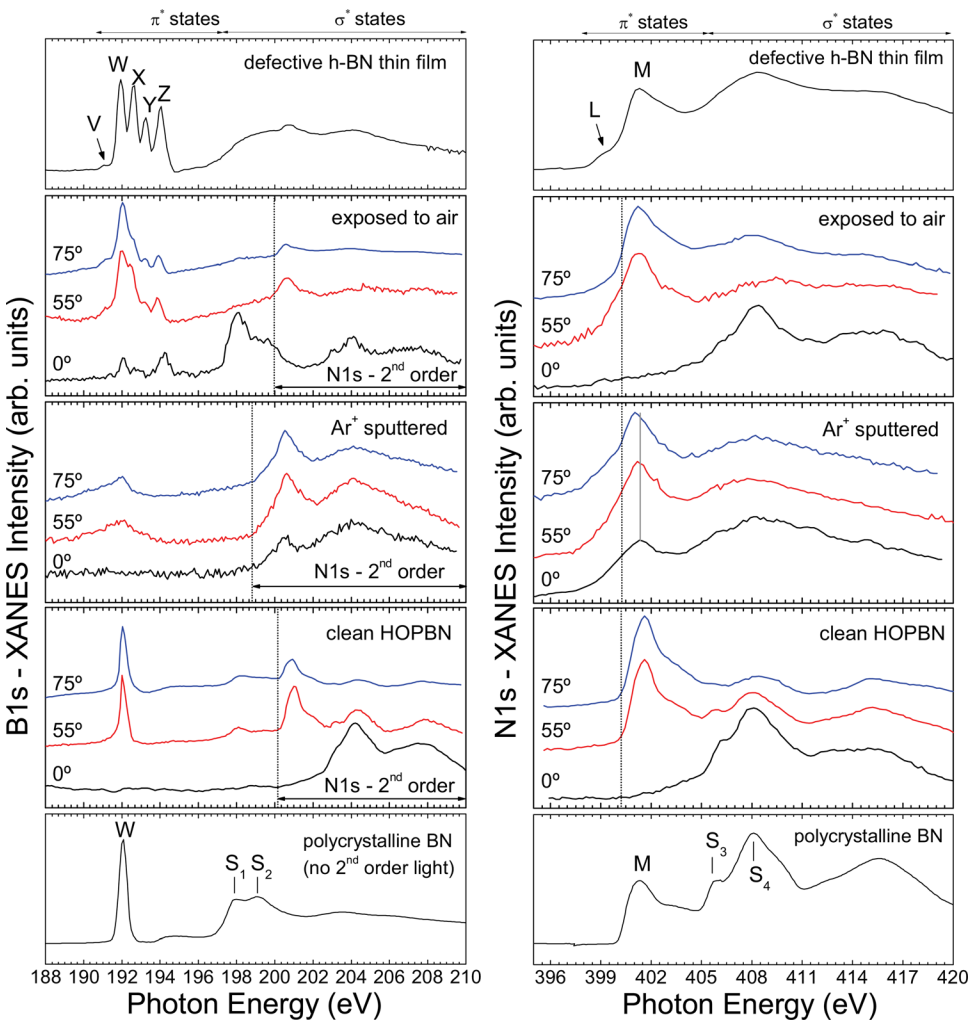

FIG. 1. (Color online) Angle-resolved B1*s* and N1*s* XANES spectra of HOPBN measured in three consecutive stages: (a) clean sample, (b) Ar^+ sputtered in ultra-high vacuum, and (c) after subsequent air exposure. The XANES spectra of polycrystalline *h*-BN powder (bottom panels) and a defective *h*-BN thin film (top panels) are shown as references.

500 eV (top panels). The former contains all the essential XANES features of a crystalline stoichiometric *h*-BN sample and the latter represents the usual spectra of a defective *h*-BN due to ion bombardment.

All the XANES spectra of *h*-BN materials consist mainly of two regions corresponding to electron transitions from the 1*s* core level to π^* and σ^* unoccupied states. For the B1*s* absorption edge of polycrystalline *h*-BN (left bottom panel of Fig. 1), the onset of the π^* states region is at ~191.0 eV, and it is dominated by the B($1s \rightarrow \pi^*$) transition at 192.0 eV, labeled as *W*. As mentioned in the introduction, this peak is the specific fingerprint of sp^2-hybridized *B* atoms in the hexagonal *h*-BN network, i.e., a trigonal B-N_3 bonding environment. Concerning the B1*s* σ^* states, the absorption edge is located at 197.2 eV and two σ^* peaks — S_1(198.2 eV) and S_2(199.5 eV) — of different intensity are commonly observed in *h*-BN. Second order signals from the N1*s* absorption edge are also frequently detected in the B1*s* XANES spectrum unless higher x-ray diffraction orders are filtered off from the beam. The N1*s* π^* region of polycrystalline *h*-BN (right bottom panel of Fig. 1) begins at ~399.8 eV and displays an excitonic peak with the maximum centered at 401.3 eV, indicated as *M*. Moreover, depending on the degree of crystallinity, two peaks S_3(406 eV) and S_4(408.3 eV) are present in the N1*s* σ^* region, which starts at ~405 eV.

The XANES spectra of the clean HOPBN measured at the intermediate angle (55°) are qualitatively similar to the polycrystalline *h*-BN sample. However, in this case the B1*s* spectrum exhibits high N1*s* second order intensity. Besides, the N1*s* excitonic peak *M* is significantly narrower in HOPBN than in the polycrystalline *h*-BN reference, being shifted ~0.3 eV to higher energies (401.6 eV).

Both the very narrow $1s \rightarrow \pi^*$ transitions and the large π^* to σ^* intensity ratio in the B1*s* and N1*s* XANES spectra of HOPBN are indicative of a highly ordered structure. In fact, the angular dependence of the near-edge x-ray absorption of the clean HOPBN clearly confirms a perfect stacking of the basal planes parallel to the surface. Notice that at 0° incidence of the x-ray beam the electric field E is perpendicular to the p_z orbitals and hence no transition to final π^* states is allowed. Accordingly, no π^* peaks are observed at this angle neither in the B1*s* nor the N1*s* XANES spectrum of the clean HOPBN. Transitions to B1*s* σ^* states are detected, but their intensity is very weak compared to the second order N signal to which the spectrum was normalized. Rotating the sample from 0° to 75° increases the π^* intensity, since we approach the geometry at which E is parallel to p_z and the transition probability is maximum.

Additionally, it is worth mentioning that no *X-Z* peaks associated to N defects are detected in the B1*s* spectra of clean HOPBN. Also, a negligible amount of surface O was present in the clean HOPBN, as shown in Fig. 2, where the O1s XANES spectrum recorded at grazing incidence is depicted. The O1s XANES spectrum of clean HOPBN is magnified by a factor 25 to be able to see any structure of the very weak oxygen signal. We observe two peaks at 532.6 eV and 542.8 eV, labeled as A and C, which are tentatively assigned to transitions from the O1*s* core-level to π^* and σ^* states of adsorbed molecular oxygen,[55] respectively.

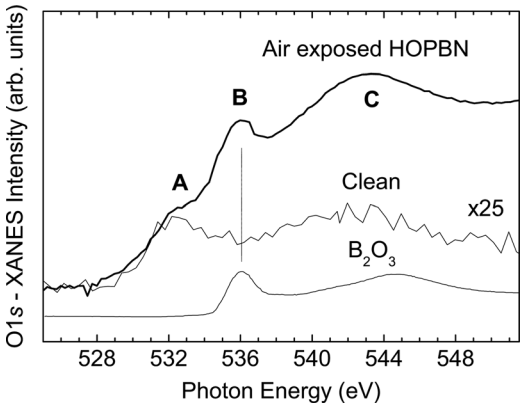

FIG. 2. Grazing incidence O1*s* XANES spectra of the clean HOPBN and the Ar^+ sputtered HOPBN exposed to air. A B_2O_3 reference spectrum from Ref. 56 is depicted for comparison purposes.

After sputtering the sample with Ar^+ (See Fig. 1), some interesting changes occur in the HOPBN structure. The intensity of the B1*s* π^* peak decreases and consist now of a broad distribution in the 188.5–194.5 eV energy range, with a maximum centered at the *W* peak position. Besides, the B1*s* σ^* edge is now hardly detected. These changes are due to the amorphization effect linked to the ion bombardment of the HOPBN surface. The spreading and reduction of B1*s* π^* states is in principle connected with the creation of N vacancies in the hexagonal BN network due to ion-atom collisions, which breaks the π bonding continuity of the material and gives rise to new B bonding environments. Furthermore, the amorphization of the sample considerably lowers its conductivity, and larger charge effects where noticeable during the measurements. For this reason, the overall intensity and the signal to noise ratio of the spectra has significantly decreased.

Notably, since the *X-Z* peaks are not present in the B1*s* XANES spectrum of HOPBN after bombardment in ultrahigh vacuum, they cannot be assigned to N vacancies. Surprisingly, regardless of the amorphization effect, the B1*s* XANES angular dependence is still consistent with the parallel stacking of basal planes in HOPBN after Ar^+ sputtering. Indeed, no B1*s* π^* states are detected at normal incidence, and peak *W* is maximum at 75°. However, the XANES angle dependence is lost for the N1*s* signal. This suggests that N atoms are displaced from the *h*-BN positions, while B atoms retain the original HOPBN hexagonal order.

Concerning the N1*s* XANES spectra, a considerable broadening of the π^* density of states is also observed after Ar^+ bombardment, and the onset of the π^* absorption edge moves down to 397.5 eV. Additionally, peak *M* shifts from 401.3 eV to 401.0 eV as we increase the angle between the sample normal and the x-ray beam. Furthermore, new π^* states are detected at the left of peak *M*, which are similar to peak *L* in the reference sample grown by PLD (N1*s* top panel). Jiménez *et al.*,[26] and recent studies by Petravic and coworkers,[39–41] have claimed that this peak is due to localized states associated to interstitial nitrogen. As mentioned before, the intense N1*s* π^* peak observed at 0° indicates the existence of randomly oriented N-B_3 environments. Finally, the amorphization effect of bombardment is assessed by the

coalescence of the S_3 and S_4 peaks, which is a typical effect in non-crystalline *h*-BN thin films.

In the last step of our experiment, the analysis of the XANES spectra acquired after exposure of the sputtered HOPBN surface to air yields some clear indications. When compared with the B1*s* XANES spectrum of the defective thin film reference on the top panel, the B1*s* π^* excitonic states of HOPBN show the formation of *X*-*Z* peaks under air exposure. Peak *V*, which has been previously reported in some cases of N_2^+ bombarded *h*-BN,[26] is also detected. Since these peaks only showed up after exposure of HOPBN to air, this suggests that both *V* and *X*-*Z* peaks originate from substitutional O or OH species in N-vacancy-related defects, and not from empty N vacancies or highly coordinated B atoms, like it has been previously suggested in literature. In agreement with this, Fig. 2 shows an intense O1s XANES signal after exposure to air of the sputtered HOPBN surface. Apart from the previously discussed A and C features, a new peak B is observed at 536.1 eV ascribed to B-O π^* states (see B_2O_3 spectrum from Ref. 56). This confirms that oxygen is incorporated to the HOPBN surface through coordination to B atoms.

Additionally, the original XANES angular dependence of the clean HOPBN, with its hexagonal planes parallel to the surface, is almost completely recovered (except for a small signal intensity detected in the π^* states region of B1*s* and N1*s* at 0° incidence). Apparently, oxygen serves in the restoration of the hexagonal BN structure, suggesting that nitrogen vacancies considerably retained the hexagonal order. In this respect, theoretical calculations yielded a very small distortion of the structure around a N vacancy after relaxation of the three B atoms around it in *h*-BN.[48] As we shall discuss later in more detail, only the intensity variation of peaks *V* and *W* is consistent with a perfect stacking of the basal planes parallel to the surface, while peaks *X*-*Z* slightly deviate from this geometry. In any case, a large spontaneous reorganization of the HOPBN structure is clearly observed by XANES owing to interaction with reactive oxygen in the air, either molecular or in the form of water vapor.

More significantly, the N1*s* XANES spectral shape and angular dependence of the original clean HOPBN is nearly fully restored after air exposure of the ion damaged HOPBN surface. Besides, there is a large intensity decrease of the N1*s* signal in second order consistent with the loss of nitrogen. No spectral evidence of either N-O binding or other oxygen-related peaks is found in the N1*s* XANES spectra as a result of air exposure. Moreover, there is a shift of the N1*s* π^* absorption edge to higher energies and an almost complete disappearance of the *L* states assigned to interstitial nitrogen. This suggests a process of *N*-vacancy/*N*-interstitial recombination to a regular atomic site in the hexagonal BN lattice, what would also explain the intensity increase of peak *W*.

B. A core-level shift model for the B(1s→ π^*) excitonic transitions in defective hexagonal BN

In the previous section, we demonstrated that four new excitonic transitions (labeled *V* and *X*-*Z*) appear around peak *W* in the B1*s* x-ray absorption edge of HOPBN after a procedure of Ar^+ ion bombardment followed by air exposure. Among them, we will first deal with peaks *X*-*Z*, since they are most commonly observed in the XANES spectra of *h*-BN materials.

As already mentioned, peak *W* is the characteristic XANES feature of *h*-BN from sp^2-hybridized B bonded to 3 N atoms. The other peaks *X*-*Z* are due to the loss of 1, 2 or 3 N ligands, respectively. However, the results of last section have proved that interaction with air is essential to observe these peaks in the XANES spectra, suggesting an oxygen decoration mechanism of the N vacancies accompanied by a N vacancy-interstitial recombination that reconstruct the hexagonal structure damaged by ion bombardment.

The question now is whether or not a chemical shift due to O substitution of the N vacancies can account for the energy positions of peaks *X*-*Z* with respect to *W*. A first hint is found in the last $1s\rightarrow\pi^*$ transition or peak *Z*. In the opening work of Jiménez *et al.*,[25,26] peak *Z* was ascribed to elemental B-B bonds on the basis of a similar peak detected at the same energy in the B1*s* XANES spectra of elemental B and B_4C. However, this peak is now known to be caused by surface oxygen contamination and it disappears, for instance, in oxygen free B_4C after proper annealing.[57] In fact, the energy of peak *Z* coincides with the characteristic exciton of B_2O_3 from a B-O_3 bonding environment. Therefore, it seems plausible that peaks *X* and *Y* are due to intermediate situations between a B-N_3 and a B-O_3 environment, i.e., B-N_2O and B-NO_2, respectively. Supporting this hypothesis, the reported B1s binding energies for *h*-BN and B_2O_3, determined by x-ray photoemission spectroscopy (XPS), are ~191 eV (Ref. 37) and ~193.4 eV,[58,59] suggesting a core-level shift per O substituted N of ~0.8 eV that is close to the relative energy displacements of *X*-*Z* peaks.

Therefore, assuming that peak *X* (192.6 eV) arises from one substitutional O defect in *h*-BN we can state that:

$$B^{hex}+3\Delta N = 192.0\ \text{eV} \tag{1}$$

$$B^{hex}+2\Delta N+\Delta O = 192.6\ \text{eV}, \tag{2}$$

where B^{hex} refers to the binding energy of elemental B in a hypothetical hexagonal structure, while ΔN and ΔO correspond to the energy shift per N and O atomic ligand. Notice, that it is not possible to establish the binding energy of 1*s* core-level electrons by XANES. However, chemical shifts of the B1*s* core level due to substitutional O will reflect similar energy displacements of the corresponding $1s\rightarrow\pi^*$ transitions with respect to peak *W* in the XANES spectra. Indeed, from Eqs. (1) and (2) we get: ΔO-ΔN = 0.6 eV, whatever the binding energy of B1*s*.

Core-level shifts are due to the charge transfer associated to each atomic ligand, which is itself related to the difference in electronegativity of the corresponding atoms. Thus, we can consider, to a first approximation, that the energy shift per ligand is proportional to the difference in Pauling electronegativity (Δχ) of the atoms involved, divided by the total number of bonds (N_b) formed:

$$\left.\begin{array}{l}\Delta N \propto \Delta\chi^{BN}/N_b \\ \Delta O \propto \Delta\chi^{BO}/N_b\end{array}\right\} (\Delta\chi^{BN}=1, \Delta\chi^{BO}=1.4) \rightarrow \Delta O = 1.4\Delta N \tag{3}$$

From Eqs. (1)–(3) we obtain $\Delta N = 1.5$ eV, $\Delta O = 2.1$ eV and $B^{hex} = 187.5$ eV. From these values, the energy positions of the B1*s* π* resonant transitions assigned to B-N_3, B-N_2O, B-NO_2 and B-O_3 bonding environments (*W*-*Z* peaks) are 192.0 eV, 192.6 eV, 193.2 eV and 193.8 eV, respectively. The B^{hex} value is similar to the B1*s* XPS binding energy of other B materials consisting of icosahedral units, such as elemental B and B_4C (~187.7 eV (Ref. 58) and ~188.2 eV,[59] respectively). Moreover, the energy difference between the reported B1*s* XPS binding energy of B_2O_3 and elemental B is 193.4 eV − 187.7 eV = 5.7 eV, what yields a rough estimation of 1.9 eV for the core-level shift per O ligand. Similarly, an energy shift per N ligand of 1.1 eV is obtained from comparison of B and *h*-BN B1*s* XPS binding energies. Significantly, there is a reasonable agreement between these XPS-derived core-level shifts per N and O ligand and those attained from Eqs. (1)–(3).

The experimental position of peak *Z* (194.0 eV) is displaced ~0.2 eV from the energy given by the above calculation for B-O_3 coordination (193.8 eV). This is due to the fact that the complete O substitution of N vacancies to give a B-O_3 bonding environment constitutes itself the formation of a new material, B_2O_3, whose bonding geometry is not hexagonal. This also explains the different behavior of peak *Z* reported by Jiménez *et al.*[26] with respect to the other peaks in the B1s excitonic structure.

At this point, the origin of peak *V* can also be explored. Until now, we have only considered those B bonding environments that arise from the complete occupancy of N vacancies by O species. Here, we tentatively assign peak V to lower coordinated B sites with one or more N vacant sites from either a lack of or an incomplete oxygen substitution. In this sense, theoretical calculations[48] predict the formation of a half empty localized level at ~191.4 eV within the theoretical bandgap of 4 eV, induce by a neutral N vacancy in *h*-BN [considering a valence-band maximum of ~187.5 eV for *h*-BN (Ref. 60)].

C. Angular XANES study of O substitutional defects in HOPBN

In Fig. 3, we are shown the B1*s* XANES spectra of HOPBN after ion bombardment and air exposure for the different incident angles of the x-ray beam. In order to extract information about the orientation of O substitutional defects, the deconvolution of the B1*s* π* states into peaks *V*-*Z* has been carried out. The intensity of peaks *V*-*Z* for each orientation is depicted in Fig. 4. Peaks *V*, *W*, *X* and *Y* exhibit a monotonic increase of the intensity with a maximum at grazing incidence, meaning that the associated bonding environments preserve the original HOPBN orientation parallel to the surface. This supports the incorporation of O as planar sp^2-bonded tricoordinated O^+, as it was recently reported in a HRTEM study.[50] In contrast, the approximately constant intensity of peak *Z* indicates a random orientation of the B-O_3 environment. The detection of a minor intensity for all peaks at normal incidence indicates that a fraction of these bonding environments are not aligned parallel to the substrate as consequence of the ion bombardment amorphization process. Moreover, the angle independence of peak *Z* intensity suggests that this bonding environment is not part of the HOPBN planar structure and is only present in this remaining amorphous portion of the material. Notice that this peak *Z* arises from boron oxide, and as mentioned before in the text, this actually corresponds to the formation of a new material, whose crystal structure is not hexagonal.

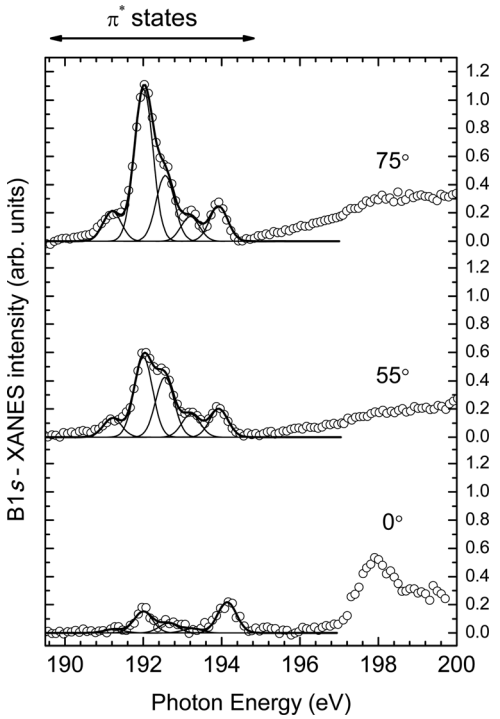

FIG. 3. Deconvolution into five Gaussian components (solid lines) of the B($1s \rightarrow \pi^*$) XANES excitonic transitions (dots) recorded at 0°, 55° and 75° incidence after air exposure of the Ar^+ sputtered HOPBN sample.

From the relative intensity of π* peaks in the angle-independent XANES spectrum measured at 55° a total oxygen substitution of [O]~30% is obtained, where $[O] = (1/3) \cdot I_X + (2/3) \cdot I_Y + I_Z$ and I_i refers to the intensity of each peak ($i = V$, X, Y and Z) normalized to the total intensity of π* peaks.

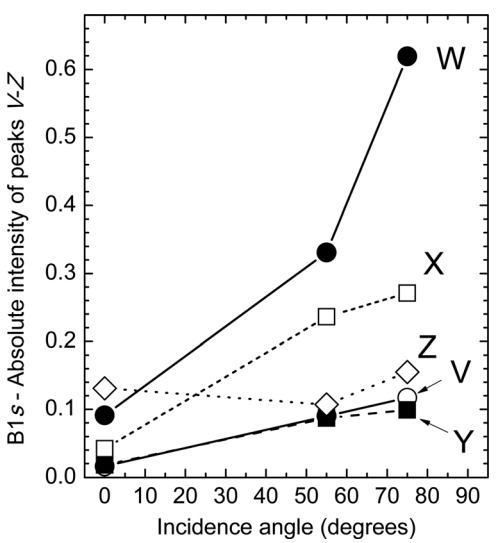

FIG. 4. Angle dependence of the intensity of peaks *V*-*Z* observed in the Ar^+ sputtered HOPBN sample after air exposure.

D. Oxygen defects in hexagonal BC and BCN compounds

Following the same argument as for *h*-BN, we can explain the origin of the four B1*s* π^* excitonic peaks previously reported in our XANES study of a hexagonal BC_3 compound grown by B and C co-evaporation.[45] Those peaks, labeled as B_0, B_1, B_3 and B_4, were detected at 189.7 eV, 191.0 eV, 192.4 eV and 194.0 eV, and attributed to 0, 1, 2 or 3 carbon vacancies in an sp^2 boron carbide structure, respectively. Again, based on: (1) the identical energy of the fourth peak B_4 and the B_2O_3 characteristic exciton, and (2) the similar energy of B_0 and the intense peak at 190.1 eV reported in the electron energy-loss spectrum of BC_3, we state that B_0, B_1, B_3 and B_4 arise from a gradually defective B bonding environment, where the C vacancies have been decorated by surface O contamination. Then, based on the core-level shift model presented here, it follows that:

$$B^{hex} + 3\Delta O = 193.8 \text{ eV} \quad (4)$$

$$B^{hex} + 2\Delta O + \Delta C = 192.4 \text{ eV}, \quad (5)$$

$$(\Delta\chi^{BC} = 0.5, \Delta\chi^{BO} = 1.4) \rightarrow \Delta O = 2.8\Delta C \quad (6)$$

Solving this system of equations we get: $\Delta C = 0.8$ eV, $\Delta O = 2.2$ eV and $B^{hex} = 187.2$ eV. Notice that these values are very similar to the ones obtained for *h*-BN, confirming the assignation of the energy displacements to substitutional O. Analogous to the *h*-BN case, we can now calculate the energy position of the four bonding environments (B_0, B_1, B_3 and B_4) corresponding to the substitution of C by O in a trigonal bonding structure. We obtain that the excitonic peaks assigned to B-C_3, B-C_2O, B-CO_2 and B-O_3 are expected at 189.6 eV, 191.0 eV, 192.4 eV and 193.8 eV, respectively. This result is consistent with the experimental position of the π^* peaks observed in the B1*s* XANES spectrum of *h*-BC_3 (Ref. 45).

Finally, we can extend this analysis to ternary BCN thin film compounds. The four B1*s* XANES spectra of samples with compositions $BC_{0.25}N$, BCN, BC_2N and BC_4N are depicted in Fig. 5. To understand these spectra, we have included carbon to the core-level shift model of the B1*s* π^* resonant structure of *h*-BN. In this way, we obtain a first scheme of the possible bonding environments of the B atoms in a hexagonal BCN compound, and the resultant energies of the B($1s \rightarrow \pi^*$) transitions in the XANES spectrum. We have chosen the *h*-BN results as starting point because this approach is consistent with the idea that a hexagonal BC_xN compound is formed by incorporation of C into the hexagonal BN network. Therefore, including the binding energy of a C atom ($\Delta C = 0.8$ eV) to the values obtained for *h*-BN we have: $B^{hex} = 187.5$ eV, $\Delta C = 0.8$ eV, $\Delta N = 1.5$ eV, $\Delta O = 2.1$ eV. According to the core-level shift model, and discarding the formation of B – B bonds, there exist ten possible bonding environments of B, three of which almost coincide in energy (See Table I). This means that the B1*s* XANES spectrum of *h*-BC_xN compounds should consist of seven different peaks.

Indeed, Fig. 5 shows that at least seven Gaussian functions are needed for the deconvolution of the B1*s* π^* states of BC_xN films. These Gaussian functions, labeled as B_0-B_6,

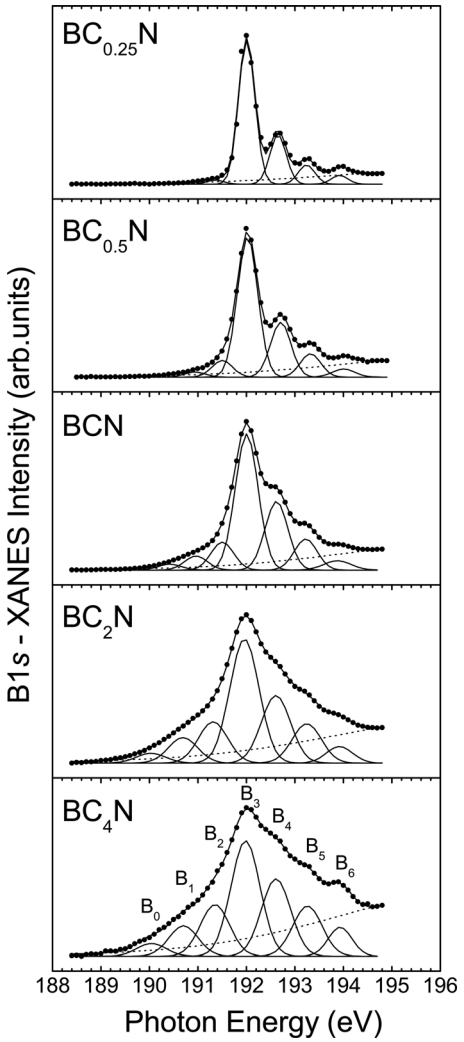

FIG. 5. Deconvolution into seven Gaussian components (solid lines) of the B($1s \rightarrow \pi^*$) XANES excitonic transitions (dots) of BC_xN ($0 < x < 4$) thin films recorded at 55° incidence.

TABLE I. Energy position of B($1s \rightarrow \pi^*$) XANES transitions assigned to different sp^2-boron bonding environments in BC_xN compounds.

sp^2-boron environment	Core-level shift model (eV)	Apparent peak position (eV)[a]
B-C_3	189.9	190.1 ± 0.1
B-C_2N	190.6	190.77 ± 0.06
B-CN_2	191.2	191.38 ± 0.04
B-OC_2	191.3	
B-CNO	191.9	191.98 ± 0.02
B-N_3	192.0	
B-O_2C	192.5	192.62 ± 0.02
B-ON_2	192.6	
B-O_2N	193.2	193.26 ± 0.02
B-O_3	193.8	193.9 ± 0.02

[a]From deconvolution of B1*s* π^* states in Fig. 5.

are centered at the energies given in Table I. These values are in good agreement with the predictions of the core-level shift model previously mentioned. We observe that the increase of C in the BCN films produces new features below 192.0 eV, which in fact correspond to the C related B bonding environments. Moreover, the broadening of the spectra suggests a reduction of the short-range order and an amorphization of the material due to the incorporation of C atoms. This is supported by an increasing defect concentration in the BCN structure, as confirmed by the increasing intensity of peaks assigned to oxygen decorated defects, mostly at energies above 192.0 eV. Recently, Petravic and coworkers[39–41] reported B1*s* XANES spectra of Ar^+ and N_2^+ bombarded *h*-BN powders attached to a conductive C tape, which are very similar to our spectra of BC_xN films with a high C content in Fig. 3. This suggests that the B1*s* XANES spectra published in Refs. 39–41 represent in fact a *h*-BN structure with substitutional C and O impurities arising from the unintentional bombardment of the carbon tape.

IV. CONCLUSIONS

In this work, we have investigated by XANES the formation and origin of point defects in a HOPBN sample, with the basal planes parallel to the surface, that was subject to Ar^+ bombardment (in ultrahigh vacuum environment) and subsequent air exposure. The results indicate a significant amorphization of HOPBN due to the impinging energetic Ar^+ ions, which preferentially sputter N atoms to create N vacant sites and interstitials. After exposure to air, the hexagonal order and orientation of HOPBN is almost fully restored through O substitutional defects incorporated into the generated N vacancies, and through recombination of N interstitials and N vacancies. No apparent features from B vacancies or interstitials were detected in any of the XANES spectra.

Furthermore, strong evidence is given throughout the article that the three extra excitonic peaks [*X* (192.6 eV), *Y* (193.2 eV) and *Z*(194.0 eV)] commonly observed in the π^* region of the B1*s* XANES spectra of hexagonal and hexagonal-like BN materials arise from the chemical shift induced by 1, 2 or 3 oxygen substitutional defects occupying N vacancies in the hexagonal lattice. Accordingly, three B bonding environments due to O impurities are detected (B-N_2O, B-NO_2 and B-O_3). The B-N_2O and B-NO_2 environments preserve a planar stacking as part of the BN sheets in HOPBN, while B-O_3 shows a random orientation.

A core-level shift model based on the different electronegativities of the atomic ligands coordinating B has been presented, which successfully accounts for the energy position of XANES peaks *V*-*Z*. This method can be applied to any other boron-based hexagonal material. We have actually proved it useful for the case of hexagonal BC_3 and BC_xN ($0 < x < 4$) compounds.

ACKNOWLEDGMENTS

We would like to thank Phillipe Parent and Carine Laffon (Université Pierre et Marie Curie, France) for providing the HOPBN sample from A. W. Moore (Union Carbide), and for their assistance at LURE. We are indebted to A. Vollmer for her help at the Optics beamline (SURICAT endstation) of the Helmholtz-Zentrum Berlin - Electron storage ring BESSY II. The research leading to these results has received funding from the European Community's Seventh Framework Programme (FP7/2007-2013) under Grant No. °226716. This work has been partially financed by the Spanish MICINN through project Consolider FUNCOAT CSD2008-0023, and project MOCASIN MAT-2010-21070-C02-02. I. Caretti acknowledges support from CSIC through a JAE-Doc Fellowship.

[1]K. Watanabe, T. Taniguchi, and H. Kanda, Nature Mater. **3**, 404 (2004), and references therein.
[2]S. N. Grinyaev, F. V. Konusov, V. V. Lopatin, and L. N. Shiyan, Phys. Solid State **46**, 435 (2004).
[3]Y. Kubota, K. Watanabe, O. Tsuda, and T. Taniguchi, Science **317**, 932 (2007).
[4]T. Taniguchi and K. Watanabe, J. Cryst. Growth **303**, 525 (2007).
[5]M. G. Silly, P. Jaffrennou, J. Barjon, J. S. Lauret, F. Ducastelle, A. Loiseau, E. Obraztsova, B. Attal-Tretout, and E. Rosencher, Phys. Rev. B **75**, 085205 (2007).
[6]P. Gevko, L. Bulusheva, A. Okotrub, V. Koroteev, I. Yushina, L. Bresson, and A. Loiseau, Phys. Status Solidi B **245**, 2107 (2008).
[7]L. Museur, D. Anglos, J. P. Petitet, J. P. Michel, and A. V. Kanaev, J. Lumin. **127**, 595 (2007).
[8]L. Museur, E. Feldbach, and A. Kanaev, Phys. Rev. B **78**, 155204 (2008).
[9]Z. L. Hou, M. S. Cao, J. Yuan, X. Y. Fang, and X. L. Shi, J. Appl. Phys. **105**, 076103 (2009).
[10]K. Nose, H. S. Yang, H. Oba, and T. Yoshida, Diamond Relat. Mater. **14**, 1960 (2005).
[11]K. Nose, H. Oba, and T. Yoshida, Appl. Phys. Lett. **89**, 112124 (2006).
[12]X. L. Chen, Y. H. Cheng, X. J. Xie, W. T. Feng, and K. Wu, J. Phys. D: Appl. Phys. **40**, 846 (2007).
[13]Y. Kubota, K. Watanabe, O. Tsuda, and T. Taniguchi, Chem. Mater. **20**, 1661 (2008).
[14]A. W. Moore, Nature **221**, 1133 (1969).
[15]S. P. S. Arya and A. Damico, Thin Solid Films **157**, 267 (1988), and references therein.
[16]Y. M. Shi, C. Hamsen, X. T. Jia, K. K. Kim, A. Reina, M. Hofmann, A. L. Hsu, K. Zhang, H. N. Li, Z. Y. Juang, M. S. Dresselhaus, L. J. Li, and J. Kong, Nano Lett. **10**, 4134 (2010).
[17]T. Thamm, W. Baumann, D. Dietrich, N. Meyer, S. Stockel, and G. Marx, Phys. Chem. Chem. Phys. **3**, 5150 (2001).
[18]J. L. Huang, C. H. Pan, and D. F. Lii, Surf. Coat. Technol. **122**, 166 (1999).
[19]B. Marlid, M. Ottosson, U. Pettersson, K. Larsson, and J. O. Carlsson, Thin Solid Films **402**, 167 (2002).
[20]K. R. Hobbs and R. D. Coombe, Thin Solid Films **402**, 162 (2002).
[21]C. L. Tsai, Y. Kobayashi, T. Akasaka, and M. Kasu, J. Cryst. Growth **311**, 3054 (2009).
[22]T. Baazi and E. J. Knystautas, Thin Solid Films **232**, 185 (1993).
[23]C. Rohr, J. H. Boo, and W. Ho, Thin Solid Films **322**, 9 (1998).
[24]K. Shinichi, T. Mari, G. Xiaoyi, K. Fumikazu, K. Saichi, and K. Mitsue, Nucl. Instrum. Methods Phys. Res. B **59**, 341 (1991).
[25]I. Jimenez, A. Jankowski, L. J. Terminello, J. A. Carlisle, D. G. J. Sutherland, G. L. Doll, J. V. Mantese, W. M. Tong, D. K. Shuh, and F. J. Himpsel, Appl. Phys. Lett. **68**, 2816 (1996).
[26]I. Jimenez, A. F. Jankowski, L. J. Terminello, D. G. J. Sutherland, J. A. Carlisle, G. L. Doll, W. M. Tong, D. K. Shuh, and F. J. Himpsel, Phys. Rev. B **55**, 12025 (1997).
[27]Y. Yap, *B-C-N Nanotubes and Related Nanostructures* (Springer, New York, NY, 2009), Vol. 6.
[28]D. Golberg, Y. Bando, C. C. Tang, and C. Y. Zhi, Adv. Mater. **19**, 2413 (2007), and references therein.
[29]C. H. Jin, F. Lin, K. Suenaga, and S. Iijima, Phys. Rev. Lett. **102**, 195505 (2009).
[30]J. C. Meyer, A. Chuvilin, G. Algara-Siller, J. Biskupek, and U. Kaiser, Nano Lett. **9**, 2683 (2009).

[31]D. Golberg, Y. Bando, O. Stephan, and K. Kurashima, Appl. Phys. Lett. **73**, 2441 (1998).
[32]P. Jaffrennou, J. Barjon, J. S. Lauret, B. Attal-Tretout, F. Ducastelle, and A. Loiseau, J. Appl. Phys. **102**, 116102 (2007).
[33]L. Museur and A. Kanaev, J. Appl. Phys. **103**, 103520 (2008).
[34]L. Museur and A. Kanaev, J. Mater. Sci. **44**, 2560 (2009).
[35]A. Katzir, J. T. Suss, A. Zunger, and A. Halperin, Phys. Rev. B **11**, 2370 (1975).
[36]A. A. Pavlychev, R. Franke, S. Bender, and J. Hormes, J. Phys.: Condens. Matter **10**, 2181 (1998).
[37]I. Shimoyama, Y. Baba, T. Sekiguchi, and K. G. Nath, J. Electron Spectrosc. Relat. Phenom. **137**, 573 (2004).
[38]I. Shimoyama, Y. Baba, T. Sekiguchi, and K. G. Nath, J. Electron Spectrosc. Relat. Phenom. **175**, 6 (2009).
[39]A. Bozanic, M. Petravic, L. J. Fan, Y. W. Yang, and Y. Chen, Chem. Phys. Lett. **472**, 190 (2009).
[40]R. Peter, A. Bozanic, M. Petravic, Y. Chen, L. J. Fan, and Y. W. Yang, J. Appl. Phys. **106**, 083523 (2009).
[41]M. Petravic, R. Peter, L. J. Fan, Y. W. Yang, and Y. Chen, Nucl. Instrum. Methods Phys. Res. A **619**, 94 (2010).
[42]T. Hemraj-Benny, S. Banerjee, S. Sambasivan, D. A. Fischer, W. Q. Han, J. A. Misewich, and S. S. Wong, Phys. Chem. Chem. Phys. **7**, 1103 (2005).
[43]H. C. Choi, S. Y. Bae, W. S. Jang, J. Park, H. J. Song, and H. J. Shin, J. Phys. Chem. B **109**, 7007 (2005).
[44]A. B. Preobrajenski, M. L. Ng, N. A. Vinogradov, A. S. Vinogradov, E. Lundgren, A. Mikkelsen, and N. Martensson, Nano Lett. **9**, 2780 (2009).
[45]I. Caretti, R. Gago, J. M. Albella, and I. Jimenez, Phys. Rev. B **77**, 174109 (2008).
[46]M. A. Mannan, T. Kida, H. Noguchi, M. Nagano, I. Shimoyama, N. Hirao, and Y. Baba, J. Ceram. Soc. Jpn. **117**, 503 (2009).
[47]M. A. Mannan, H. Noguchi, T. Kida, M. Nagano, N. Hirao, and Y. Baba, Thin Solid Films **518**, 4163 (2010).
[48]W. Orellana and H. Chacham, Phys. Rev. B **63**, 125205 (2001).
[49]S. Azevedo, J. R. Kaschny, C. M. C. de Castilho, and F. D. Mota, Nanotechnology **18**, 495707 (2007).
[50]O. L. Krivanek, M. F. Chisholm, V. Nicolosi, T. J. Pennycook, G. J. Corbin, N. Dellby, M. F. Murfitt, C. S. Own, Z. S. Szilagyi, M. P. Oxley, S. T. Pantelides, and S. J. Pennycook, Nature **464**, 571 (2010).
[51]N. Alem, R. Erni, C. Kisielowski, M. D. Rossell, W. Gannett, and A. Zettl, Phys. Rev. B **80**, 155425 (2009).
[52]J. Moscovici, G. Loupias, P. Parent, and G. Tourillon, J. Phys. Chem. Solids **57**, 1159 (1996).
[53]I. Caretti, N. Fanegas, Z. Martin, R. Torres, and I. Jimenez, J. Anal. At. Spectrom. **25**, 150 (2010).
[54]I. Caretti, I. Jimenez, and J. M. Albella, Diamond Relat. Mater. **12**, 1079 (2003).
[55]J. G. Chen, Surf. Sci. Rep. **30**, 1 (1997).
[56]Y. Muramatsu, H. Takenaka, T. Oyama, T. Hayashi, M. M. Grush, and R. C. C. Perera, X-Ray Spectrom. **28**, 503 (1999).
[57]I. Jimenez, D. G. J. Sutherland, T. van Buuren, J. A. Carlisle, L. J. Terminello, and F. J. Himpsel, Phys. Rev. B **57**, 13167 (1998).
[58]C. W. Ong, H. Huang, B. Zheng, R. W. M. Kwok, Y. Y. Hui, and W. M. Lau, J. Appl. Phys. **95**, 3527 (2004), and references therein.
[59]M. M. Ennaceur and B. Terreault, J. Nucl. Mater. **280**, 33 (2000).
[60]J. B. MacNaughton, A. Moewes, R. G. Wilks, X. T. Zhou, T. K. Sham, T. Taniguchi, K. Watanabe, C. Y. Chan, W. J. Zhang, I. Bello, S. T. Lee, and H. Hofsass, Phys. Rev. B **72**, 195113 (2005).